



## Torsional strength analysis of universal joint's ZP-11A due to yokes modification and materials

Hartono Yudo<sup>a</sup>, Andi Setiawan<sup>a, \*</sup>, Ocid Mursid<sup>a</sup>, Muhammad Iqbal<sup>b</sup>

<sup>a</sup> Department of Naval Architecture, Faculty of Engineering, Diponegoro University  
Jl. Prof. Sudarto No.13, Semarang, 50275, Indonesia

<sup>b</sup> Department of Naval Architecture, Ocean, and Marine Engineering, University of Strathclyde  
100 Montrose Street, Glasgow G4 0LZ, United Kingdom

Received 7 July 2022; 1<sup>st</sup> revision 5 October 2022; 2<sup>nd</sup> revision 8 October 2022; 3<sup>rd</sup> revision 10 October 2022; 4<sup>th</sup> revision 14 October 2022;  
Accepted 17 October 2022; Published online 29 December 2022

### Abstract

The study examined the strength of the universal joint after it was loaded with torsion. It used different materials that can withstand tensile stress in accordance with accepted principles and made modifications to the yoke as a result of the topology optimization process. The topology optimization determined that the yoke's part needed to withstand load without changing its dimensions and minimize stress distribution. According to the results, the maximum shear stress on the spider of the original universal joint model made of JIS-SF590A steel was 84.57 MPa, the shear stress on the yoke component was 30.84 MPa, and the maximum von Mises was 341.1 MPa. As a result of using JIS-SF590A steel, yoke modification 3 has produced a reduction in shear stress of 12.97 % and a reduction in von Mises stress of 35.33 % from the original yoke. This is the most efficient design of yoke and also this modified yoke form provides a wider elevation angle and is easier to manufacture.

Copyright ©2022 National Research and Innovation Agency. This is an open access article under the CC BY-NC-SA license (<https://creativecommons.org/licenses/by-nc-sa/4.0/>).

Keywords: shear stress; topology optimization; universal joint; von mises.

### I. Introduction

The azimuth thruster system, commonly known as the Z-Peller, is a propulsion system that is mounted vertically and has a 3600 degrees rotation. Their nozzle concentrates the water flowing around the blades. J. C. Kim *et al.* [1] looked into the maneuverability of the azimuth thruster system on the research vessel. Because of its capacity to rotate 3600, the Z-peller system has remarkably high maneuverability and efficiency. Some studies were carried out to study the material optimization of the steering yoke. The original universal joint and the modified universal joint with topology optimization were compared and evaluated in A. Koparde *et al.* [2] studied with the help of finite element software. The results showed that the modified yoke provided a uniform distribution across the entire structure. This resulted in a reduction of the maximum stress by 22.9 % and a mass reduction of the yoke by 22.4 %

when compared to the original yoke. The failure might be brought on by unfavorable factors, including the environment, bad planning, or unstable torque loading. According to the study by NS Giridhar *et al.* [3], strong materials were selected and component dimensions were changed to reduce component stress and weight. The mechanism has the advantage of becoming simple to manufacture because it is constructed from two distinct sheet metals. Numerous mechanisms with various dimensions are created. Strong evidence suggests that the steel variant. The intricate driving motion transmission consists of a long shaft with Cardan joints with variable geometry mounted on each end. The study by Chaban *et al.* provides a system of ordinary differential equations with a combined issue of Dirichlet first-type and Poincaré third-type boundary conditions is utilized to represent non-linear electromechanical differential equations [4].

The stress concentration can be reduced by fillet, but the amount of fillet provided should be optimum. Pastukhov *et al.* [5] using the WinShaft module in APM WinMachine, shaft design justification, and test computations are executed based on CAE tools. To

\* Corresponding Author. Phone: +62-85156236032  
E-mail address: andisetiawaan213@gmail.com

decrease speed variations between the input and output shafts, the U-joints are arranged in a Z-configuration. The study by Bharti *et al.* is established that the Sommerfeld phenomenon, which is defined by resonance capture and escape by resonance, exists for significant parallel offsets between the input and output shafts. The escape by resonance is followed by a rapid increase in speed and a decrease in the amplitude of the torsional vibration. In reality, these jump phenomena happen at two separate speed ranges, one close to the inherent frequency of the U-joints' straight-line arrangement and the other at half of it. The rate at which the input shaft torque or power is changed has an impact on the dynamic response's nature [6]. The universal joint components as shown in Figure 1.

Zbigniew *et al.* [7] discovered that the elastic moment model might replicate true transient processes in the joint coordinates of the system by employing the fractional derivative integrator. Furthermore, it provides accuracy on par with the model with dispersed parameters. A modified Hamilton-Ostrogradski concept is implemented to create shaft equations, which are then utilized to analyze both the fully coupled system and the distributed parameter system. It is utilized to calculate rotational angles of shaft elements and essential analytical mechanics functions of the velocity continuum. Popena *et al.* [8] investigated how the transmission shaft interacts between the working mechanism and the driving motor. The study by Ekemb *et al.* approaches relies on analogies among mechanical and electrical systems. For the aforementioned transmission shaft, the equivalent circuits that are customary in electrical systems are defined. Long and flexible shafts, which are a regular feature of synchronous motors used in LCI technology, are extremely vulnerable to torsional vibration excite when their resonant frequency combine with any external load exerted on the shaft. International standards require a torsional analysis to assess the shaft's durability across the motor's entire speed range. Therefore, for such an evaluation, the motor air gap torque's frequency and magnitude are necessary [9].

The dynamic characteristics of a viscous-spring damper utilized to regulate the torsional vibration of the engine's shaft system, as well as the vibration characteristics of an ultra-long-stroke engine using de-rating technology, are reviewed in this study. Jaehoon *et al.* [10] recommended that the assigned

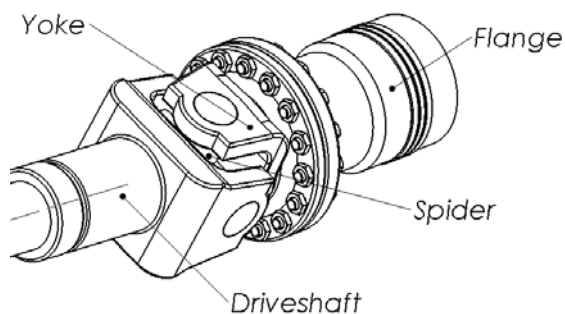


Figure 1. Universal joint components

probabilities for attempting to control torsional vibration in the propulsion shafting system would have to include adapting the design parameters of its dampening effect instead of using the optimum damper designed from concept to prevent fatigue fracture of shafts, in scenarios where ships have recently witnessed an engine acceleration issue in the critical zone. The Stribeck friction curve is applied to estimate the friction force between the shaft and the water-lubricated rubber bearing. Then, by using the modal synthesis method of substructures, the modal shapes of the shaft and the hull are integrated through the friction force to establish the nonlinear differential system of equations of the shaft-hull coupled system. After that, the self-excited vibration responses carried on by friction can be computed using the Runge-Kutta method to solve the nonlinear differential governing equations. On this base, the study by Wu *et al.* are held regarding how the friction coefficient, damping ratio, rotation speed, and support stiffness affect the shaft-hull coupled system's self-excited vibration. The results demonstrated that the difficulty of the shaft-hull coupled system's self-excited vibration would increase as damping, shaft speed of rotation, or supporting stiffness [11]. The poles encounter both shear and torsional force as a result of the forces that are applied to them. Vehicles' motion transmission mechanisms are made up of a few sections, some of which occasionally encounter severe disappointments. A rotating part is generated when forces combine, and this section is vulnerable to fragility because of fluctuating torque. The two most important components of a car are the steering mechanism and the steering column. It is a critical element for achieving the vehicle's security and steady development. It has poles that have been shaped into a cross in the center of the roadway and had loads on each of its poles that were attached in the same manner as a cross joints. It experiences torsion force in adding to shear force as a result of forces placed on the cross-joint poles. Vehicles' movement transmission systems are formed of a few parts, some of which can suffer severe disappointments [12].

According to the study of Cardoso *et al.* [13], the manufacturing process and material design, specifically the amount, location, and roughness of mechanical stakes and forks, as well as the content of microstructure inclusions, are variables that could affect fatigue life in this automobile component. A computer-aided multibody modeling approach for the simulation of a Cardan joint with manufacturing errors was studied by Cirelli *et al.* [14]. During the modeling phase, the elasticity of flexible bodies is lumped and the joint compliance is taken into account using concentrated non-linear spring elements. The torsional fluctuations in the flexible coupling dramatically increased and then abruptly ceased. The coupling connected to the intermediate shaft did not have sufficient radial flexibility to dampen these vibrations.

The study of Song *et al.* [15] concluded that to avoid the effects of the self-excited torsional vibration, it is recommended that this coupling is

Table 1.  
Dimension of Universal Joint Assembly

Part	Dimension
Shaft diameter	130 mm
Universal joint length	1100 mm
Universal joint diameter	260 mm
Elevation angle	5.73°
Bolt type	M20 x 2.5 x 80
Flange length	381.5 mm
Flange outside diameter	350 mm

replaced with one that is capable of absorbing the radial shaft displacement. Investigation of a parallel manipulator with Cardan and prismatic joints was studied by Pugi *et al.* [16]. It is recommended that the layout involves a relatively stiff and robust structure. The manipulator is supposed to be moved by direct-drive linear actuators. This choice is justified by the possibility of accurate control of heavy insertion losses. This is done by simplifying or removing a large part of the additional actuation and sensing systems that are normally installed on conventional machines. According to the residual threshold of the associated linear systems, both reduced-order bases are enriched, and the grid resolution is adaptively determined based on the relative inaccuracy in approximating the objective function and constraint values throughout the iteration. With acceptable goal and constraint violation errors, the tests on benchmark 2D and 3D show increased performance. The impact of important stress constraint factors, thus the allowable stress value, stress penalty factor, and p-norm factor, is carefully examined by Xiao *et al.* [17].

The gradients necessary to carry out the optimization could be computed relatively fast using the adjoint approach. Gregor *et al.* [18] have successfully derived the gradients using a "first optimize then discretize" scheme. By enhancing the topology both of hard and soft magnetic thin film structures, the method's capabilities are proven, and

the outcomes are confirmed by comparison with an analytical solution. References from previous studies and cases of mechanical failures involving universal joints are provided. Using ship shaft data, one may perform a static analysis of a universal joint to calculate the shear stress, von Mises, and safety factor. The yoke should be optimized by static simulations with a variety of materials that fulfill the tensile strength requirement rule. Due to modifications in the form of the yoke and the material used to construct it, we will analyze the torsion strength of the universal joint.

## II. Materials and Methods

### A. Data

To examine this study, the universal joint assembly model should be created. Before doing an analysis, the dimensions of the universal joint components should be determined. The dimensions of the universal joint assembly used in this study are shown in Table 1.

### B. Material variations

JIS-SF590A was chosen as a material for the original yoke. Based on the BKI rule, we will use other materials for variation of materials in this study, where materials for shafting components must have a tensile strength of 400-800 MPa, as shown in Table 2.

### C. Yoke variations

The yoke component makes an elevation angle at installation possibly. The modification of the yoke shape is considered to result in a reduced yoke mass, make manufacturing easier, and increase the elevation angle of installation. The yoke variations that will be applied involve modifying the original ship yoke shape. This will involve several modified yoke forms based on the topology optimization results and another yoke form from the previous study. The yoke variations are shown in Figure 2.

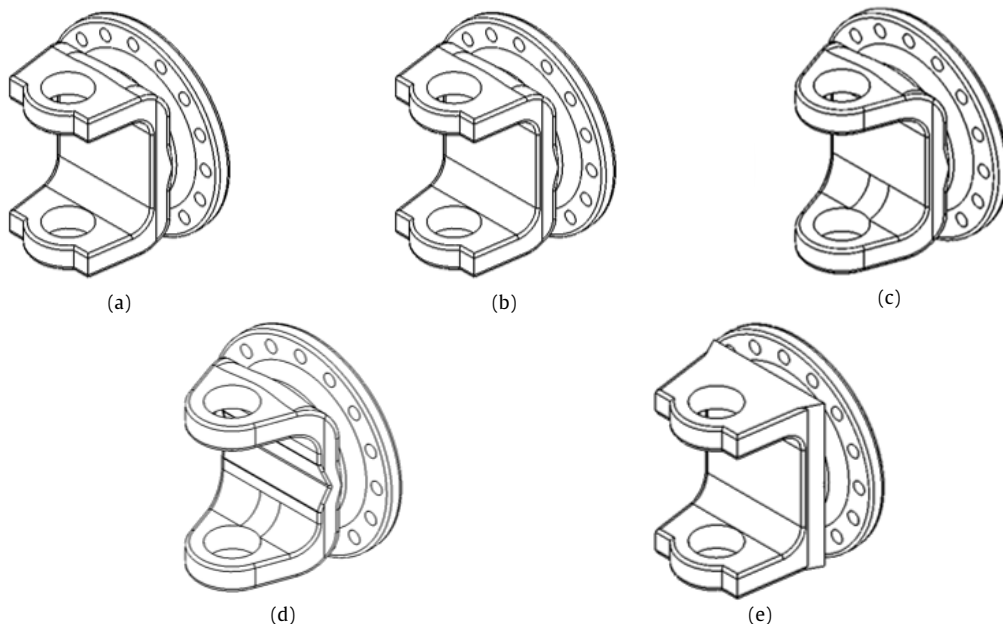


Figure 2. The yoke variations: (a) original yoke; (b) yoke modification 1; (c) yoke modification 2; (d) yoke modification 3; (e) yoke modification 4

Table 2.  
Material's mechanical properties

Mechanical properties	ASTM A36	JIS-SF590A	AISI Stainless Steel 316L	SS41 (bolt-nut)
Tensile strength	400 MPa	590 MPa	485 MPa	475 MPa
Yield strength	250 MPa	295 MPa	170 MPa	225 MPa
Density	7,850 kg.m-3	7,800 kg.m-3	8,000 kg.m-3	7,800 kg.m-3
Poisson ratio	0.26	0.29	0.3	0.3
Elastic modulus	200 GPa	200 GPa	173 GPa	210 GPa

The design of Figure 2(a) shows the default yoke installed on the tug boat, for the shape of the yoke in design modification 3 in Figure 2(c) looks at the results of the topology study that has been done. The modified model 4 in Figure 2(e) is based on the yoke shape in the research conducted by Y. Richard *et al.* [5]. Meanwhile, the cutting of the middle cross-section of the yoke with dimensions of 80 mm x 10 mm in Figure 2(b) and Figure 2(d) sees the distribution of low stress from the simulation results.

#### D. Boundary condition and loading condition

Using SOLIDWORKS 2020, 3D finite element model was generated. The shape of the solid meshed with tetrahedral cell technology. Tetrahedral cells are very effective for solid structures because they are flexible and adapt to irregular or curved shapes. The application will support multi-core surface and volume meshing using curvature base mesh. It is

excellent for meshing complex structures. Figure 3 shows the mesh on the model.

The torque of the main engine is calculated by dividing the power and rpm of the main engine [19]. At the flange connected to the main engine, the torque of 15,174.96 Nm was given at the flange connected to the main engine as shown in Figure 4. In addition, boundary conditions were applied at the flange connected to the intermediate shaft, as shown in Figure 5.

At the flange attached to the intermediate shaft, all motions were fixed. Static structural analysis was carried out using SOLIDWORKS 2020 solver.

#### E. Mesh convergence

Mesh convergence is a method for comparing the most stable results for each element size from several stress analysis results with various element sizes. The convergence is carried out to evaluate the

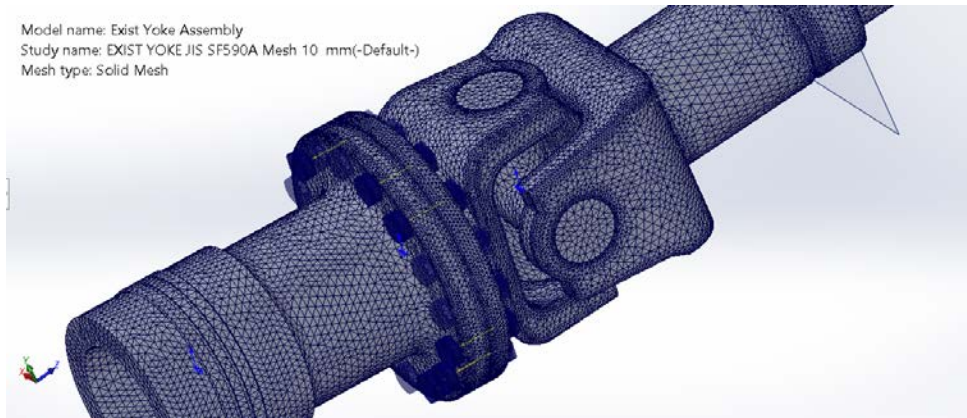


Figure 3. Meshing of model

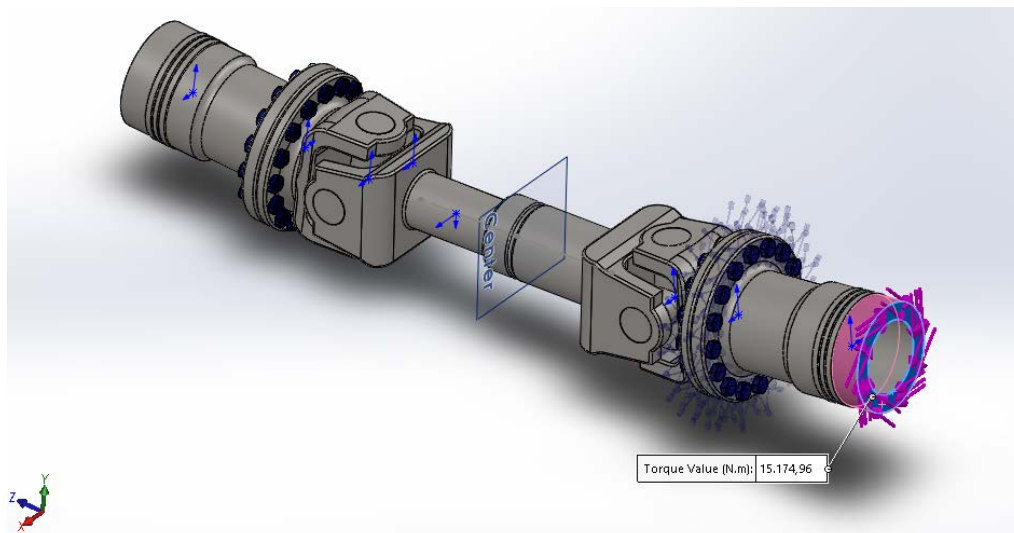


Figure 4. Apply moment torque location

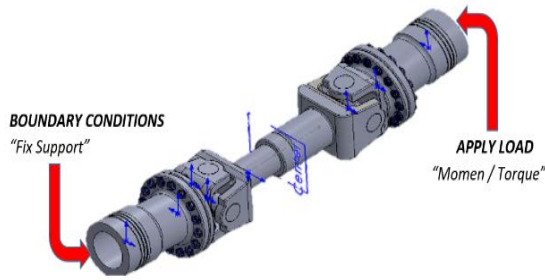


Figure 5. Boundary condition and moment location

software's precision. Figure 6 shows the convergence of the mesh elements. At meshing diameters between 10 mm and 9 mm, mesh convergence is obtained. A meshing size of 10 m is determined with a stress value of 84.55 MPa based on the convergence results.

### III. Results and Discussions

#### A. Topology optimization of the original yoke

The optimization of the yoke is discovered using the topology optimization method. This method offers the most efficient material layout for design and loading. The SOLIDWORKS 2020 Topology Optimization Study was used to observe the element density distribution for the original yoke and identify the low-stress regions shown in Figure 7.

The low-stress areas that can be eliminated by paying attention to manufacturing lines, as well as certain functional constraints are shown in Figure 7.

The dead zone, as seen in the blue area, is where components from that region do not contribute to the workload and, therefore, can be eliminated. It must remain in the yellow area because it is required to withstand the workload placed on the models.

#### B. Simulation result on the original yoke of universal joint

The torque of the main engine is calculated by dividing the power and rpm of the main engine [19]. At the flange connected to the main engine, the torque of 15,174.96 Nm was given and the component was analyzed for the strength of the models. From the simulation results using the software, the largest values of shear stress and von Mises stress are obtained. In the ship's universal joint assembly model using JIS-SF590A material, the maximum shear stress is 84.57 Mpa, located on the spider shown in Figure 8. The shear stress on the yoke is 30.84 MPa and the maximum von Mises stress is 341.1 MPa located on the yoke, as shown in Figure 9.

#### C. Simulation result on the yoke modifications

##### 1) Comparison of shear stress result

The modified yoke was analyzed for the same boundary conditions, and shear stress and von Mises stress results were observed. The shear stress and von Mises distribution of the modified yoke are shown in Figure 10 and Figure 11, respectively.

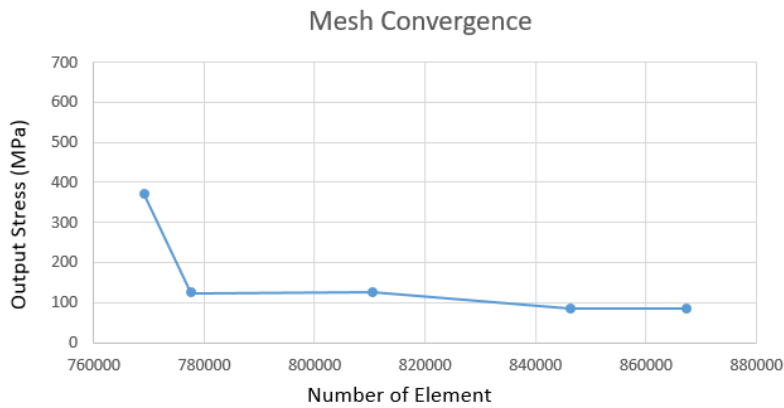


Figure 6. Graph of mesh convergence

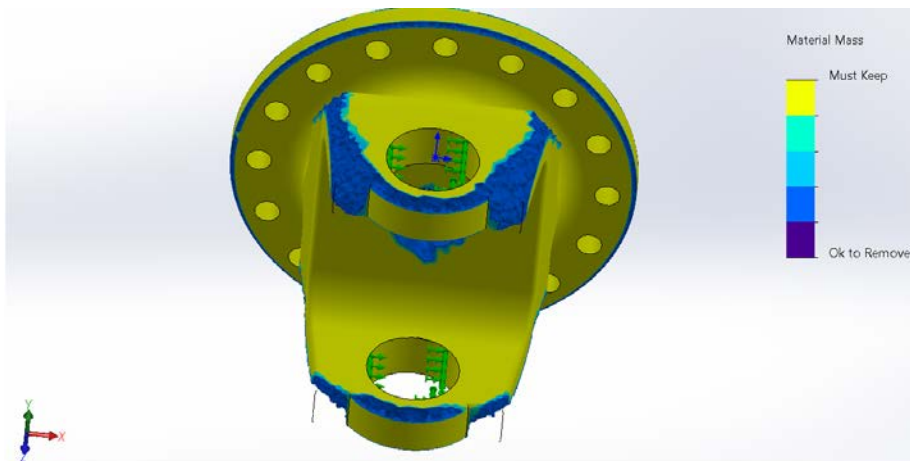


Figure 7. Yoke topology study

The critical point in each model variation lies in the spider component. The shear stress results from

static simulation for each model variation are presented in Table 3, Table 4 and Table 5. The

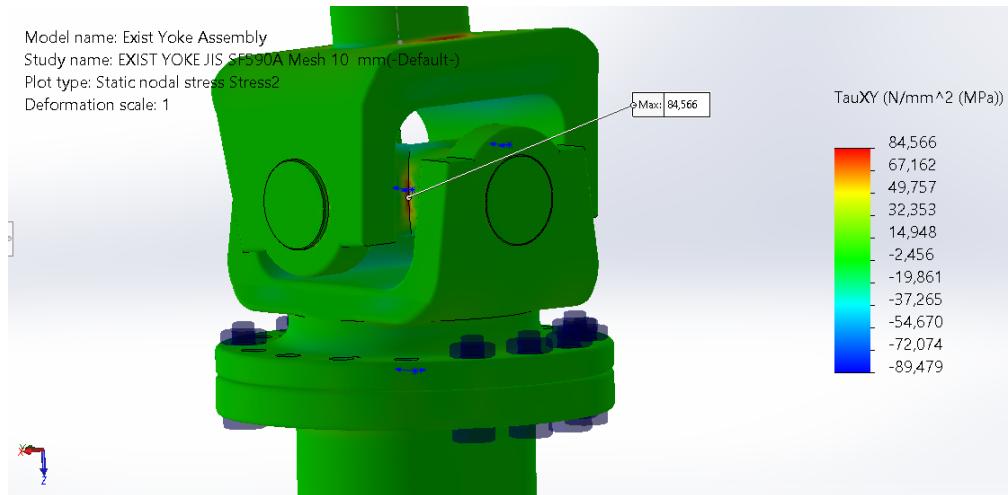


Figure 8. The simulation analysis results of shear stress on the original universal joint

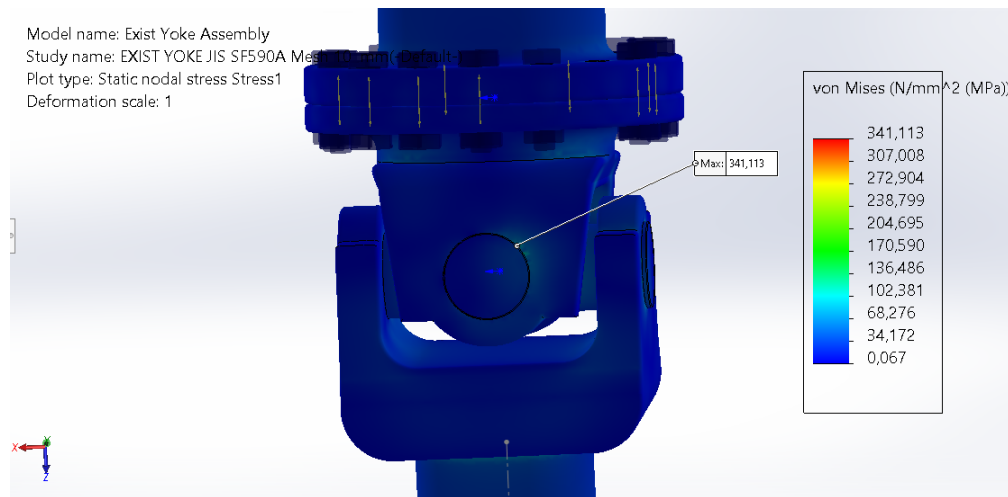


Figure 9. The simulation analysis results of von Mises on the original universal joint

Table 3. Comparison of shear stress of each model with ASTM A36 steel

Model	Yoke (MPa)	Spider (MPa)	Driveshaft (MPa)	Flange (MPa)
Original yoke model	29.1	85.64	42.42	20.17
Yoke modification 1	28.44	84.96	86.75	20.28
Yoke modification 2	27.32	84.84	41.69	20.15
Yoke modification 3	27.13	84.89	38.54	20.28
Yoke modification 4	27.92	84.79	85.35	20.15

Table 4. Comparison of shear stress of each model with JIS-SF590A steel

Model	Yoke (MPa)	Spider (MPa)	Driveshaft (MPa)	Flange (MPa)
Original yoke model	30.84	84.57	43.33	21.05
Yoke modification 1	28.08	84.63	85.85	21.3
Yoke modification 2	27.03	84.52	41.36	21.04
Yoke modification 3	26.84	84.56	38.45	21.29
Yoke modification 4	27.63	84.47	84.54	21.04

Table 5. Comparison of shear stress of each model with AISI Stainless Steel 316L

Model	Yoke (MPa)	Spider (MPa)	Driveshaft (MPa)	Flange (MPa)
Original yoke model	29.37	84.84	42.41	20.31
Yoke modification 1	28.38	84.91	86.6	20.45
Yoke modification 2	27.27	84.79	41.68	20.3
Yoke modification 3	27.01	84.84	38.53	20.3
Yoke modification 4	27.87	84.74	85.22	20.3

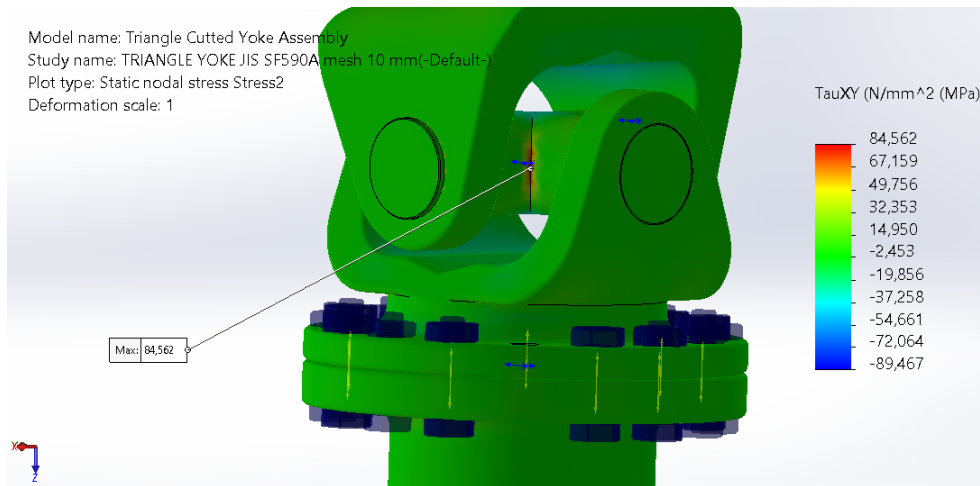


Figure 10. The simulation analysis results of shear stress on the modified yoke

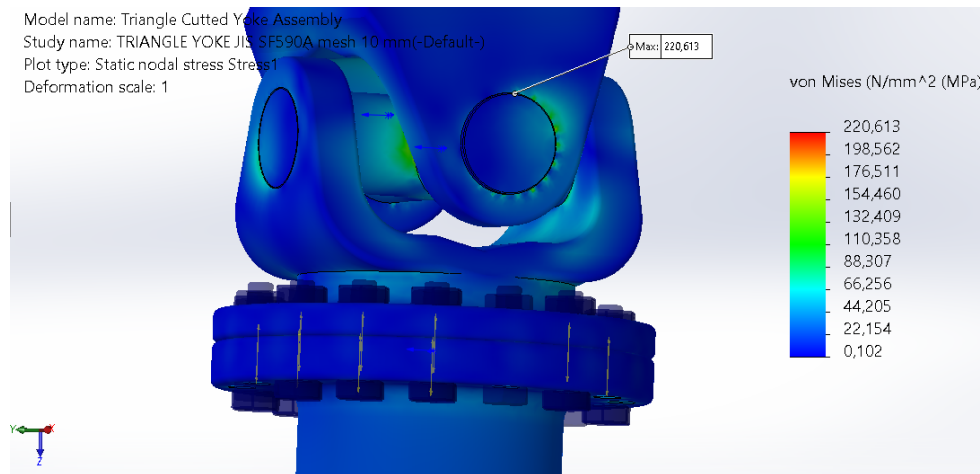


Figure 11. The simulation analysis results of von Mises on the modifies yoke

maximum shear stress obtained using the model's variation is significantly below the ASTM A36 material's yield strength 250 MPa. The reduction of shear stress on the yoke is 6.77 % compared with the original yoke, as shown in the modified model of yoke 3.

The maximum stress obtained in the model variation is significantly lower than the 295 MPa yield strength of the JIS-SF590A material. The shear stress on the yoke of the modified model 3 has been reduced by 12.97 %. The maximum stress obtained in the model variation is significantly lower than 170 MPa yield strength for AISI Stainless Steel 316L material. The shear stress reduction on the yoke is 8.035 %, which can be seen in the modified model of yoke 3.

The results obtained by numerical analysis of the stress distribution at the input yoke of the universal joint showed that even small variations in shape could cause significant variations in the stress distribution. Therefore, topology optimization is carried out to obtain the efficiency of stress distribution on the yoke. The case with the lowest voltage level is identified and selected as the most profitable design solution. Based on the shear stress analysis results from all the variations presented, the yoke modification 3 with JIS-SF590A steel has the greatest stress reduction compared to other variations, amounting to 12.97 %.

## 2) Comparison of von Mises result

The critical point of von Mises stress in each variation model lies in the eye pad of the yoke component. The results of von Mises stress simulation results for each model variation are presented in Table 6, Table 7, and Table 8.

The von Mises stress has been reduced by 34.81 % using the modified model of yoke 3 compared to the ship's original yoke. It can be seen that when compared to the ship's original yoke, the modified yoke 3 model has 35.33 % von Mises stress reduction.

Compared to the ship's original yoke, the redesigned model of yoke 3 has a 34.20 % lower von Mises stress. The results of the numerical analysis of the stress distribution at the universal joint's input yoke revealed that even minor shape changes may result in significant modifications in the stress distribution. The yoke modification 3 with JIS-SF590A steel has the greatest stress reduction compared to other variations, equal to 35.33 %, based on the von Mises stress analysis results from all the variants shown.

## 3) Comparison of safety factors

The safety factor criteria for universal joint components based on the BKI rule that applies to main shafting components is 1 [20]. The safety factor

Table 6.  
Comparison of von Mises stress of each model with ASTM A36 steel

Model	Yoke (MPa)	Spider (MPa)	Driveshaft (MPa)	Flange (MPa)
Original yoke model	348.8	184.8	173.1	53.81
Yoke modification 1	229.3	184.9	157.3	53.9
Yoke modification 2	351.1	184.7	150.3	54.8
Yoke modification 3	227.4	184.7	155.9	53.89
Yoke modification 4	277.1	184.2	149.8	53.81

Table 7.  
Comparison of von Mises stress of each model with JIS-SF590A steel

Model	Yoke (MPa)	Spider (MPa)	Driveshaft (MPa)	Flange (MPa)
Original yoke model	341.1	181.9	172.1	53.5
Yoke modification 1	222.9	182	156.2	53.57
Yoke modification 2	338.5	181.8	150	53.49
Yoke modification 3	220.6	181.8	155.5	53.56
Yoke modification 4	270.5	181.8	149.9	53.5

Table 8.  
Comparison of von Mises stress of each model with AISI Stainless Steel 316L

Model	Yoke (MPa)	Spider (MPa)	Driveshaft (MPa)	Flange (MPa)
Original yoke model	344.2	184.3	172.9	53.76
Yoke modification 1	228.3	184.4	157.3	53.85
Yoke modification 2	249.2	184.2	150.2	53.75
Yoke modification 3	226.5	184.2	124.5	53.83
Yoke modification 4	276.2	184.2	149.9	53.75

calculation can be obtained compared to the yield strength of the material with the results of von Mises stress must be higher than 1 [19]. Components like the yoke, spider, and driveshaft of universal joints must comply with that safety factor criteria. Figure 12 shows the yoke safety factor data for each

model. It is known that only modifications 1, 3, and 4, manufactured with JIS-SF590A material, as well as modifications model 3 manufactured of ASTM A36, are yoke components that fulfill the safety factor criteria. Figure 13 shows the spider safety factor. Only the original yoke model and the variations of

Safety Factor Comparison of Yoke for each Materials

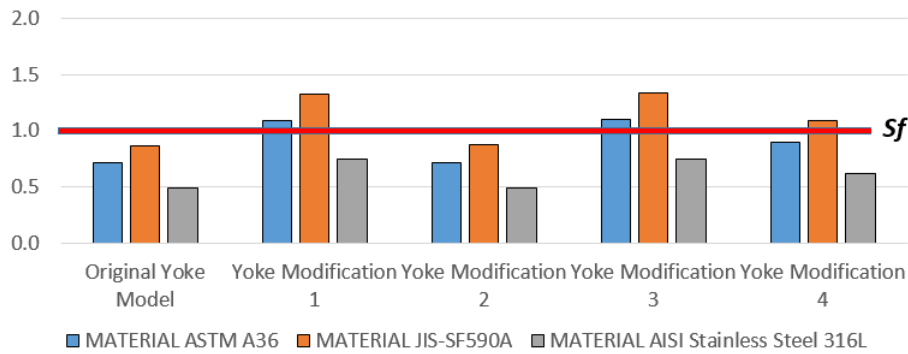


Figure 12. Graph of yoke component safety factor with several materials

Safety Factor Comparison of Spider for each Materials

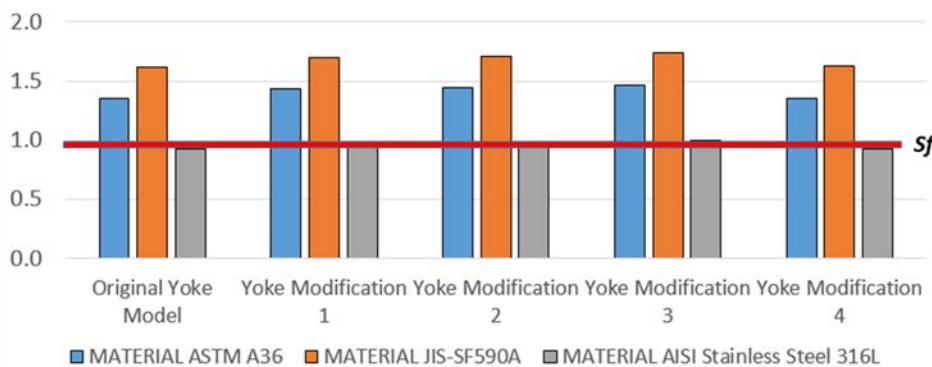


Figure 13. Graph of spider component safety factor with several materials

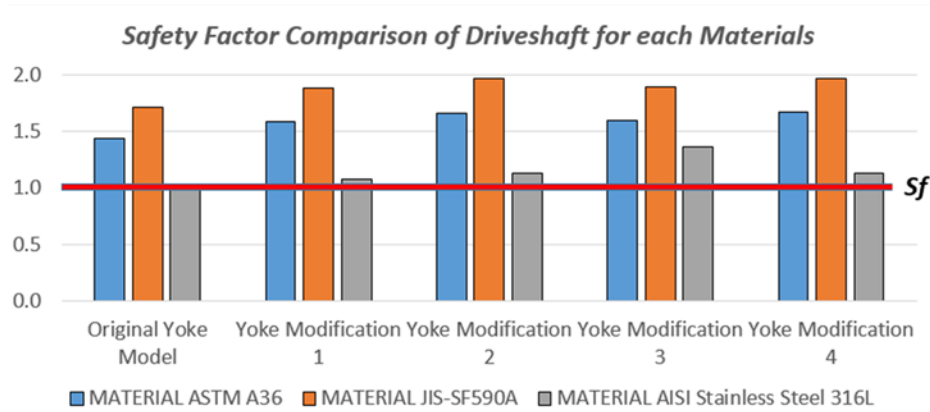


Figure 14. Graph of driveshaft component safety factor with several materials

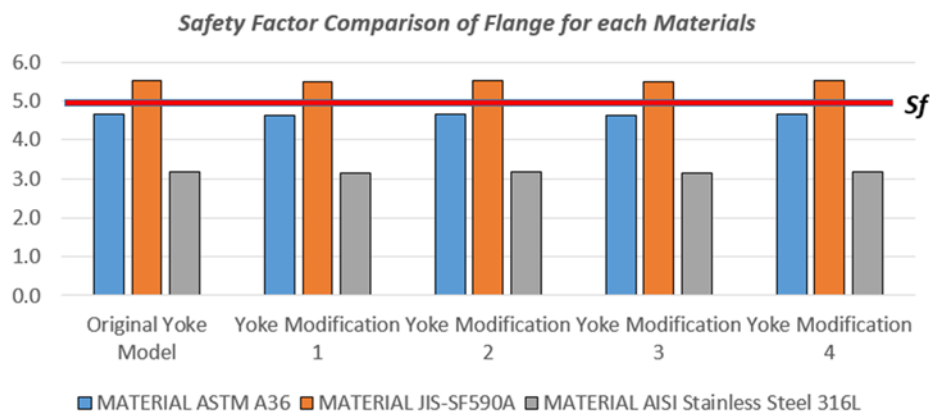


Figure 15. Graph of flange component safety factor with several materials

yoke modification with AISI Stainless Steel 316L are the spider components that do not fulfill the safety factor criteria. Figure 14 shows the driveshaft safety factor. According to the BKI rule, which applies to main shafting components, the safety factor requirement for universal joint components is 5 [20]. It can be seen that the flange components comply with the safety factor criteria for all models. Figure 15 shows the results of the safety factor of the flange for each model.

#### IV. Conclusion

Based on the analysis results, it can be concluded that the JIS-SF590A material used in the ship's universal joint model has maximum shear stress of 30.84 MPa and a von Mises stress of 341.1 MPa, which is found on the eye yoke pad. The original yoke will obtain the element density of stress distribution by topology optimization. In the modified yoke 3 models, there is a reduction of 35.33 % in von Mises and 12.97 % in the shear stress of the yoke component, respectively. Each universal joint component made of ASTM A36 and JIS-SF590A materials has fulfilled the safety factor criteria. The modified yoke 3 has a very good shape in terms of strength because it has minimal stress. Its design also provides a greater elevation angle than the original ship yoke model, making it easier to manufacture and install.

#### Acknowledgments

This research is supported by Department of Naval Architecture, Faculty of Engineering, Diponegoro University, Semarang, Indonesia. We are also immensely grateful to all researcher who is joined in this research.

#### Declaration

##### Author contribution

Andi Setiawan: Writing & Editing, Conceptualization, Formal analysis, Investigation, Resources, Visualization. Hartono Yudo, Ocid Mursid, and Muhammad Iqbal: Review & Editing, Supervision

##### Funding statement

This research did not receive any specific grant from funding agencies in the public, commercial, or not-for-profit sectors.

##### Competing interest

The authors declare that they have no known competing financial interests or personal relationships that could have appeared to influence the work reported in this paper.

##### Additional information

Reprints and permission: information is available at <https://mev.lipi.go.id/>.

Publisher's Note: National Research and Innovation Agency (BRIN) remains neutral with regard to jurisdictional claims in published maps and institutional affiliations.

## References

- [1] J.C. Kim, I.K. Kang, J.H. Lee, S.J. Ham, C.W. Park, and S.H. Kim, "The maneuvering characteristics of the research vessel NARA equipped with the azimuth thruster system," *J. Korean Soc. Fish. Technol.*, vol. 53, no. 3, pp. 276–285, 2017.
- [2] A. Koparde, N. Mithra, and S. Ahankari, "Numerical and experimental analysis of torsional stress of traditional and modified steering yoke," *Mater. Today Proc.*, vol. 46, pp. 7099–7104, 2021.
- [3] N. S. Giridhar, S. Hetawal, and P. Baskar, "Finite element analysis of universal joint and propeller shaft assembly," vol. 5, no. 5, pp. 226–229, 2013.
- [4] A. Chaban, Z. Łukasik, A. Popena, and A. Szafraniec, "Mathematical modelling of transient processes in an asynchronous drive with a long shaft including cardan joints," *Energies*, vol. 14, no. 18, 2021.
- [5] A. Lozynskyy, A. Chaban, T. Perzyński, A. Szafraniec, and L. Kasha, "Application of fractional-order calculus to improve the mathematical model of a two-mass system with a long shaft," *Energies*, vol. 14, no. 7, 2021.
- [6] S. K. Bharti and A. K. Samantaray, "Resonant capture and Sommerfeld effect due to torsional vibrations in a double Cardan joint driveline," *Commun. Nonlinear Sci. Numer. Simul.*, vol. 97, p. 105728, 2021.
- [7] Ł. Zbigniew, C. Andriy, S. Andrzej, and Ż. Woźodymyr, "Model matematyczny układu napędowego z silnikiem asynchronicznym i pompą pionową," *Prz. Elektrotechniczny*, vol. 94, no. 1, pp. 133–138, 2018.
- [8] A. Popena, M. Lis, M. Nowak, and K. Blecharz, "Mathematical modelling of drive system with an elastic coupling based on formal analogy between the transmission shaft and the electric transmission line," *Energies*, vol. 13, no. 5, 2020.
- [9] G. Ekemb, F. Slaoui-hasnaoui, J. Song-manguelle, P. M. Lingom, and I. Fofana, "Instantaneous electromagnetic torque components in synchronous motors fed by load-commutated inverters," *Energies*, vol. 14, no. 11, 2021.
- [10] J. Jee, C. Kim, and Y. Kim, "Design improvement of a viscous-spring damper for controlling torsional vibration in a propulsion shafting system with an engine acceleration problem," *J. Mar. Sci. Eng.*, vol. 8, no. 6, 2020.
- [11] C. Wu, F. Chen, and X. Long, "The self-excited vibration induced by friction of the shaft-hull coupled system with the water-lubricated rubber bearing and its stick-slip phenomenon," *Ocean Eng.*, vol. 198, p. 107002, 2020.
- [12] A. Kohli, M. Hombalmath, A. Y. Patil, and P. C. Aruna Kumara, "Analysis of universal joint using virtual simulation method," *Mater. Today Proc.*, vol. 59, pp. 858–866, 2022.
- [13] A. S. M. Cardoso et al., "Fatigue resistance performance of universal cardan joint for automotive application," *Eng. Fail. Anal.*, vol. 135, no. February, p. 106128, 2022.
- [14] M. Cirelli, V. Rossi, P. P. Valentini, and E. Pennestri, "A dynamic model of a Cardan joint to evaluate the effect of elasticity and manufacturing errors," *Int. J. Veh. Perform.*, vol. 7, no. 1–2, pp. 136–155, 2021.
- [15] M. Song, T. Nam, and J. Lee, "Self-excited torsional vibration in the flexible coupling of a marine propulsion shafting system employing cardan shafts," pp. 1–13, 2020.
- [16] L. Pugi, L. Fiorineschi, and F. Rotini, "Preliminary design investigation of a rprp parallel manipulator with cardan joint and direct drive actuation," *IEEE/ASME Int. Conf. Adv. Intell. Mechatronics, AIM*, vol. 2021–July, pp. 1207–1212, 2021.
- [17] M. Xiao, J. Ma, D. Lu, B. Raghavan, and W. Zhang, "Stress-constrained topology optimization using approximate reanalysis with on-the-fly reduced order modeling," *Adv. Model. Simul. Eng. Sci.*, vol. 9, no. 1, 2022.
- [18] G. Wautischer, C. Abert, F. Bruckner, F. Slanovc, and D. Suess, "A topology optimization algorithm for magnetic structures based on a hybrid FEM–BEM method utilizing the adjoint approach," *Sci. Rep.*, vol. 12, no. 1, pp. 1–11, 2022.
- [19] E. P. Popov, *Mechanics of solids*. p. 106, Prentice Hall Inc., 2nd edition, 1976.
- [20] BKI, *RULES for machinery installations edition 2021*. vol. VI, 2021.